Journal Title
XX(X):1–22

DOI: 10.1177/ToBeAssigned
www.sagepub.com/
SAGE

A novel sliding mode speed control based strategy for permanent magnet linear synchronous motors with a model predictive current control loop

Guanyang Hu[1] Tinglong Pan[1] Wentao Huang[1] Xinggang Yan[2] Weilin Yang[1] and Dezhi Xu[3]

Abstract

Model predictive control (MPC) has been widely investigated as an advanced control method for permanent magnet linear synchronous motors (PMLSMs). It is known that the computational burden is usually heavy when multi-step MPC is considered. In this paper, a computationally efficient multi-step continuous control set model predictive control approach is proposed for the current control loop of a PMLSM. A non-singular terminal sliding mode control is employed for the speed control loop to reduce the influence caused by external disturbances. In order to further improve the closed-loop control performance, a load observer is designed to estimate the load changes in real time. Simulations and experiments reveal the effectiveness of the proposed control method for PMLSMs, which facilitates practical applications.

Keywords

continuous control set model predictive control; permanent magnet linear synchronous motors; non-singular terminal sliding mode control; load observer.

[1]School of Internet of Things Engineering, Jiangnan University, Wuxi, 214122, China
[2]School of Engineering and Digital Arts, University of Kent, Canterbury, UK
[3]School of Electrical Engineering, Southeast University, Nanjing, 210096, China

Corresponding author:
Weilin Yang, School of Internet of Things Engineering, Jiangnan University, Wuxi, 214122, China.
Email: wlyang@jiangnan.edu.cn.

Prepared using sagej.cls *[Version: 2017/01/17 v1.20]*

Introduction

Permanent magnet linear synchronous motors (PMLSMs), stemming from linear motor category, possess many advantages e.g., fast speed response, accurate fast positioning, and zero-transmission characteristics. Hence, they offer low mechanical loss, large thrust density, and fast dynamic response (Yin et al. (2022); Wang et al. (2018)). Likewise, they are widely employed in military equipments and industrial production, e.g., electromagnetic catapult, computer numerical control machine tools, and maglev train etc (Shi et al. (2016); Xu et al. (2019)).

A PMLSM control system behaves as a complex nonlinear system, which usually requires sophisticated control strategies to achieve great control performance (Englert and Graichen (2018); Kommuri et al. (2021); Wang et al. (2022)). A cascade control structure is often adopted for PMLSMs control system, which includes an outer control loop to track the reference speed and an inner control loop to track the reference current, which usually has faster dynamics. The inner control loop plays an important role in the entire control system, which requires advanced control strategies to achieve precise control of PMLSMs. Nowadays, commonly used control methods for the inner loop include proportional integral (PI) control, current hysteresis control, model predictive control (MPC), and some other intelligent control methods (Chen and Liu (2017); Wang and Tsai (2017); Jon et al. (2017)).

MPC originates from process industries in 1980s, which is able to deal with multi-input multi-output control problems with constraints. Since then, it has been intensively investigated and widely used in many other applications. Recently, MPC has been considered as an effective control method in power electronics and electrical motor drives (Ahmed et al. (2017); Huang et al. (2023); Abu-Ali et al. (2022); Nguyen et al. (2021b)), due to its merits of fast responses and small ripples. According to the existence of a modulation module, the relevant MPC strategies can be divided into two categories i.e., finite control set model predictive control (FCS-MPC) (Ahmed et al. (2017); Huang et al. (2023)) and continuous control set model predictive control (CCS-MPC) (Abu-Ali et al. (2022); Nguyen et al. (2021b)). FCS-MPC has a simpler structure and lower cost in engineering applications. However, due to lack of a modulation module, the current total harmonic distortion (THD) in FCS-MPC is relatively high.

Similar to FCS-MPC, CCS-MPC is also used for a wide range of applications (Guo et al. (2021); Nguyen et al. (2021a)). For instance, a explicit model predictive speed control approach for PMSM was proposed in one reported work (Guo et al. (2021)). The proposed method combined with multi-point linearization can reduce the impact of model mismatch, which includes two parts: offline calculation and online table lookup. The former needs a special toolbox to complete, so the algorithm is more complicated and the feasibility of the method is verified only by Simulink.

Likewise in Nguyen et al. (2021a), a combination of CCS-MPC algorithm and fuzzy control algorithm was proposed and applied to a three-phase constant voltage constant frequency inverter with an output LC filter. Corresponding results indicated that the proposed method could obtain an acceptable output voltage with a better transient response, lower THD , and smaller steady-state error. The single-step CCS-MPC only

considers in Nguyen et al. (2021a), which can achieve short-term optimal control effects, and has the advantage of low computational burden. However, since the single-step predictive control algorithm ignores the state error information for a period of time in the future, it cannot guarantee that the control variables remain optimal for a period of time.

Although both the two strategies have good dynamic responses, the current ripples using CCS-MPC are usually smaller than that using FCS-MPC (Ahmed et al. (2018); Koiwa et al. (2019); Jiang et al. (2022); Siami et al. (2017)). In a word, most of the control algorithms for PMLSM are mainly based on the cascade control structure, which mainly includes a speed outer loop and two current inner loops.For the outer speed loop, the main consideration is how to reduce the impact of external disturbances. Although the classical PI control algorithm has a simple structure, its anti-disturbance capability sometimes can't meet the requirements. Therefore, some scholars have introduced the sliding mode control algorithm with strong anti-disturbance ability into the outer speed loop to improve its robustness. However, the traditional sliding mode control algorithm also has some inherent drawbacks, such as chattering and singularity, which may destroy the operating conditions of the sliding mode of the system, resulting in excessive overshoot, and even instability. To address the singular problems in general terminal sliding mode control (TSMC), a robust model-free nonsingular terminal sliding-mode control (NTSMC) method based on ultra-local model is proposed to reduce the influence of motor parameter changes on control performance in Zhao et al. (2019). However, the unknown terms in ultra-local model can only be observed by the observer, and its control performance is constrained by the performance of the observer. In addition, the author designed an ideal sliding mode surface, which contains Sign function terms and requires the controller to have an infinite Switching frequency. However, the actual control device is often not ideal and cannot achieve an infinite Switching frequency. Due to this irrational condition, the actual sliding mode motion state cannot accurately reach the pre-designed sliding mode surface, but instead travels back and forth on both sides of the sliding mode surface, which may result in severe chattering. In another work, NTSMC method was studied for PMLSM, and realized accurate position tracking (Xu et al. (2022)). While avoiding the singularity, the reported position tracking response is faster than traditional methods. during load changes.

Correspondingly, to overcome the above-mentioned problems, a novel multi-step continuous control set model predictive control approach for PMLSMs with improved speed control loop is proposed in this paper. The main contributions of this paper are summarized as follows:

(i) Firstly, CCS-MPC algorithm is used to replace PI controller in the inner loop. It not only avoids complicated parameter tuning of PI controller, but also obtains better performance. Moreover, compared to traditional CCS-MPC approaches, integration of the CCS-MPC algorithm with quadratic optimization algorithm substantially reduces the computational burden without sacrificing the optimal switch state. Although the system structure of CCS-MPC based on the quadratic

optimization is more complicated, it has many advantages compared with the FCS-MPC, i.e., less current harmonics and low computational burden.

(ii) Secondly, to mitigate the impact of disturbance, we design a controller through NTSMC approach to replace the PI controller in outer loop. Additionally, to reduce the chattering problem caused by SMC algorithm, this paper adopts a quasi sliding mode, that is, a new type of piecewise function is utilized to replace the sign function of ideal sliding mode. In addition, a nonlinear disturbance observer (NDO) is designed in this paper to compensate the time-varying loads.

(iii) Finally, the effectiveness of the proposed algorithm is verified by both simulations and experiments.

The remainder of this paper is organized as follows. Section II describes the mathematical model of PMLSMs. Likewise. Section III describes the multi-step CCS-MPC method based on the quadratic optimization method which is applied to the current control loop. A novel NTSMC approach based controller for the speed control loop is presented in Section IV. The block diagram of PMLSMs control system are shown in Fig. 1. Then, simulations and experimental results are provided in Section V to demonstrate the effectiveness of the proposed approach. In Section VI, the paper ends with some conclusions.

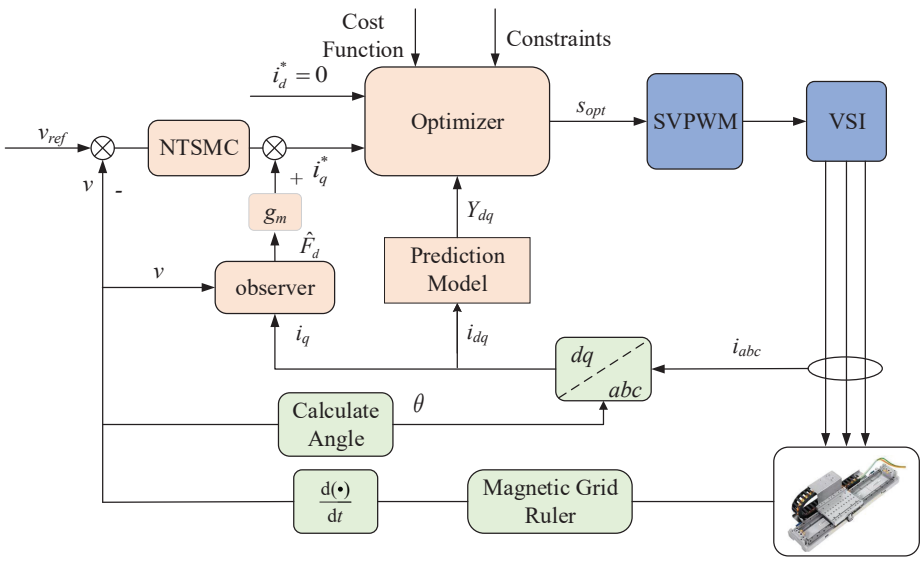

Figure 1. Block diagram of PMLSM control system using CCS-MPC strategy.

Mathematical modelling of PMLSMs

Some mild assumptions are made before presenting the PMLSM model:

(i) The saturation of motor core is ignored;
(ii) The eddy current and hysteresis losses in the motor are excluded;
(iii) The three-phase current waveform is an ideal sine wave.

Remark 1

The actual PMLSM model is a nonlinear system with strong coupling. Considering that there are many difficulties in applying model predictive control to nonlinear systems, such as large amount of computation, lack of effective solver, etc., the model is simplified in this paper.

In order to facilitate the controller design, the mathematical model of PMLSMs is established based on $d-q$ axis (Candelo-Zuluaga et al. (2021)).The relevant voltage equation is expressed as follows:

$$\begin{bmatrix} u_d \\ u_q \end{bmatrix} = R_s \begin{bmatrix} i_d \\ i_q \end{bmatrix} + \begin{bmatrix} \dot{\psi}_d \\ \dot{\psi}_q \end{bmatrix} + \omega_e \begin{bmatrix} -\psi_q \\ \psi_d \end{bmatrix}, \tag{1}$$

where u_d, u_q are the stator voltages of d axis, and q axis, respectively, and i_d, i_q are the stator currents on d axis, and q axis, respectively. Similarly, $\dot{\psi}_d$ and $\dot{\psi}_q$ are differentials for components of permanent magnet flux linkage corresponding to d axis and q axis respectively. The term, R_s represents the stator resistance and ω_e refers to electrical angular speed.

The flux equation and electromagnetic thrust equation can be written as follows:

$$\begin{bmatrix} \psi_d \\ \psi_q \end{bmatrix} = \begin{bmatrix} L_d & 0 \\ 0 & L_q \end{bmatrix} \begin{bmatrix} i_d \\ i_q \end{bmatrix} + \begin{bmatrix} \psi_f \\ 0 \end{bmatrix}, \tag{2}$$

$$F_e = K_T i_q = F_d + B_v v + M\dot{v}, \tag{3}$$

$$F_d = F_L + F_f + F_r, \tag{4}$$

where, L_d, L_q are components of inductance on $d-q$ axis respectively, ψ_f is the permanent magnet flux linkage and F_e is electromagnetic thrust. Moreover, $K_T = \frac{3}{2}\frac{\pi}{\tau} n \psi_f$ is the thrust coefficient, τ is polar distance, B_v is viscous friction coefficient, v represent the speed for PMLSM, n is number of pole pairs, and M is mover mass. F_d represents the disturbances, including load disturbances F_L, friction between the motor and the guide rail F_f and thrust fluctuations caused by end effects F_r. According to Eq. (2), Eq. (1) can be rewritten as:

$$\begin{cases} u_d = R_s i_d + L_d \frac{di_d}{dt} - \omega_e L_q i_q, \\ u_q = R_s i_q + L_q \frac{di_q}{dt} + \omega_e L_d i_d + \omega_e \psi_f. \end{cases} \tag{5}$$

In this paper, a surface-mount PMLSM is selected, which has the same inductance components under the $d-q$ axis coordinate, that is, $L_d = L_q = L$. Moreover, to facilitate decoupling, we set $i_d^* = 0$, where i_d^* is a reference current of d axis. The whole

mathematical model of PMLSMs in $d-q$ axis is summarized as follow:

$$\begin{cases} u_d = R_s i_d + L\frac{di_d}{dt} - \omega_e L i_q, \\ u_q = R_s i_q + L\frac{di_q}{dt} + \omega_e L i_d + \omega_e \psi_f, \\ F_e = \frac{3}{2}\frac{\pi}{\tau} n \psi_f i_q = F_d + B_v v + M\dot{v}. \end{cases} \tag{6}$$

CCS-MPC Schemes for the current control loop

Before presenting the relevant results on the proposed MPC scheme, the state equation of stator current is obtained first. Selecting i_d, i_q as state variables and u_d, u_q as control variables. According to Eq. (6), the state equation of stator current can be written as follow:

$$\begin{bmatrix} \frac{\mathrm{d}}{\mathrm{d}t} i_d \\ \frac{\mathrm{d}}{\mathrm{d}t} i_q \end{bmatrix} = \begin{bmatrix} -\frac{R_s}{L} & \omega_e \\ -\omega_e & -\frac{R_s}{L} \end{bmatrix} \begin{bmatrix} i_d \\ i_q \end{bmatrix} + \begin{bmatrix} \frac{1}{L} & 0 \\ 0 & \frac{1}{L} \end{bmatrix} \begin{bmatrix} u_d \\ u_q \end{bmatrix} - \begin{bmatrix} 0 \\ \frac{\omega_e \psi_f}{L} \end{bmatrix}. \tag{7}$$

A three-phase two-level voltage source inverter (VSI) has been used in this paper. It has eight switching states, including six non-zero switching states and two zero switching states. Let $s = \begin{bmatrix} \gamma_a & \gamma_b & \gamma_c \end{bmatrix}^{\mathrm{T}}$, where $\gamma_a, \gamma_b, \gamma_c$ is conducting state of the upper bridge arm of VSI, and $\gamma_a, \gamma_b, \gamma_c \in \{0, 1\}$. Values γ_a, γ_b, $\gamma_c = 1$, correspond the on-state for upper bridge arm switching device, and cut-off state for lower bridge arm switching device, and vice versa. From the principle of coordinate transformation, transformation of three-phase voltage from natural coordinate system to synchronous rotating coordinate system requires two coordinate transformations. The transformation formula is given as follows:

$$\begin{bmatrix} u_d \\ u_q \end{bmatrix} = U_{dc} G_{2/2} G_{3/2} G_m s, \tag{8}$$

where

$$G_{2/2} = \begin{bmatrix} \cos\theta & -\sin\theta \\ \sin\theta & \cos\theta \end{bmatrix}, \tag{9}$$

$$G_{3/2} = \frac{2}{3} \begin{bmatrix} 1 & -1/2 & -1/2 \\ 0 & \sqrt{3}/2 & -\sqrt{3}/2 \end{bmatrix}, \tag{10}$$

$$G_m = \frac{1}{3} \begin{bmatrix} 2 & -1 & -1 \\ -1 & 2 & -1 \\ -1 & -1 & 2 \end{bmatrix}, \tag{11}$$

s is the switching state, and U_{dc} is the DC voltage and θ is the mover position angle. Thus, the current prediction model is represented as

$$\begin{aligned} \begin{bmatrix} \frac{\mathrm{d}}{\mathrm{d}t} i_d \\ \frac{\mathrm{d}}{\mathrm{d}t} i_q \end{bmatrix} = & \begin{bmatrix} -\frac{R_s}{L} & \omega_e \\ -\omega_e & -\frac{R_s}{L} \end{bmatrix} \begin{bmatrix} i_d \\ i_q \end{bmatrix} + \begin{bmatrix} \frac{U_{dc}}{L} & 0 \\ 0 & \frac{U_{dc}}{L} \end{bmatrix} G_{2/2} G_{3/2} G_m s \\ & - \begin{bmatrix} 0 \\ \frac{\omega_e \psi_f}{L} \end{bmatrix}. \end{aligned} \tag{12}$$

Single-step CCS-MPC

To introduce the concept of multi-step prediction, we first elaborate the principle of single-step predictive control based on the discrete model. According to Euler's formula, the discrete differential form can be obtained as:

$$\begin{cases} \frac{\mathrm{d}i_d(k)}{\mathrm{d}t} \approx \frac{i_d(k+1)-i_d(k)}{T_s}, \\ \frac{\mathrm{d}i_q(k)}{\mathrm{d}t} \approx \frac{i_q(k+1)-i_q(k)}{T_s}. \end{cases} \tag{13}$$

Define the system matrices as

$$A = \begin{bmatrix} 1-\frac{T_s R_s}{L} & T_s\omega_e \\ -T_s\omega_e & 1-\frac{T_s R_s}{L} \end{bmatrix}, \tag{14}$$

$$B = \begin{bmatrix} \frac{T_s}{L} & 0 \\ 0 & \frac{T_s}{L} \end{bmatrix} U_{dc} G_{2/2} G_{3/2} G_m, \tag{15}$$

$$F = \begin{bmatrix} 0 \\ -\frac{T_s \psi_f}{L}\omega_e \end{bmatrix}, \tag{16}$$

where T_s is sampling time of control system. From Eqs. (12-16), the discretized model can be obtained as follows:

$$\begin{bmatrix} i_d(k+1) \\ i_q(k+1) \end{bmatrix} = A \begin{bmatrix} i_d(k) \\ i_q(k) \end{bmatrix} + Bs(k) + F. \tag{17}$$

Let $x_{dq} = [i_d, i_q]^T$ as the state variable, $\cdot(k+i|k)$ represents the term for time $k+i$ predicted based on time k. Thus, the one-step prediction model can be reformulated as:

$$x_{dq}(k+1|k) = Ax_{dq}(k) + Bs(k) + F. \tag{18}$$

We further define the following variables

$$\Delta x_{dq}(k+1|k) = x_{dq}(k+1|k) - x^*_{dq}(k), \tag{19}$$

$$\Delta s(k|k) = s(k) - s(k-1), \tag{20}$$

where $x^*_{dq}(k|k)$ is the reference current at time k and $\Delta s(k|k)$ represents the switching effort, which represent the change of switching state between the time k and $k-1$. $s(k-1)$ is the optimal control input at the last moment. Consequently, the cost function can be designed with the following form.

$$J = \|\Delta x_{dq}(k+1|k)\|_2^2 + \lambda \|\Delta s(k|k)\|_2^2 . \tag{21}$$

The parameter $\lambda > 0$ is a weighting factor used to adjust between the tracking accuracy of current and switching losses. Since the time delay in control system degrades the overall

performance, delay compensation need to be considered. In this paper , it is assumed that the time delay T_d is shorter than the sampling interval T_s, i.e., $T_d \leq T_s$. During the implementation, the optimal switching state $s(k)$ obtained at time k is employed at time instant $k+1$. To this end, two-step prediction of the current $x_{dq}(k+2|k)$ is considered based on $x_{dq}(k)$,

$$\begin{aligned} x_{dq}(k+2|k) =& Ax_{dq}(k+1|k) + Bs(k+1) + F \\ =& A(Ax_{dq}(k) + Bs(k-1) + F) + Bs(k+1) + F \\ =& A^2 x_{dq}(k) + ABs(k-1) + Bs(k+1) + (A+I)F. \end{aligned} \tag{22}$$

Note that in the above predictions the system matrices are assumed to be constant for simplicity. Correspondingly, the following cost function is optimized

$$J = \left\| x_{dq}(k+2|k) - x^*_{dq}(k|k) \right\|_2^2 + \lambda \left\| s(k+1) - s(k-1) \right\|_2^2. \tag{23}$$

Multi-step CCS-MPC based on quadratic optimizations

The single-step CCS-MPC only considers the optimization problem in the next time domain in the future, which can achieve short-term optimal control effects, and has the advantage of low computational burden. However, Since the single-step predictive control algorithm ignores the state error information for a period of time in the future, it cannot guarantee that the control variables remain optimal in a period of time. Compared with single-step CCS-MPC, multi-step CCS-MPC predicts state variables for multiple control period, so that it can maintain a long-term optimal state under the action of the optimal control variables. However, with the increase of predictive step, the prediction times of traditional CCS-MPC increases geometrically, which causes a large computational burden to the processor. In order to overcome the above problems, we introduce the quadratic programming algorithm into multi-step CCS-MPC, which can reduce computational burden greatly without sacrificing the optimal solution.

In this work, we implement a CCS-MPC strategy based on quadratic optimizations to avoid heavy computations in multi-step problem solving.

Define a switching sequence as follows:

$$S = [s(k), ..., s(k+N-1)]^T, \tag{24}$$

where $0 \leq |s(l)(i)| \leq 1, i = 1, 2, 3, \forall l = k, ..., k+N-1$, and N is prediction horizon length.

Assuming that the mover velocity is constant within the predictive horizon. In rolling time domain, the predictive system state value can be expressed as:

$$\begin{aligned} x_{dq}(k+N|k) = A^N x_{dq}(k) + [A^{N-1}B ... A^0 B]S \\ + [A^{N-1}F + ... + A^0 F]. \end{aligned} \tag{25}$$

Let Y_{dq} represent the predictive current output sequence within the prediction horizon (from $k+1$ to $k+N$) and ${Y^*}_{dq}$ is the corresponding reference output.

$$Y_{dq} = \Gamma x_{dq}(k) + \Upsilon S + \Pi, \tag{26}$$

where:

$$\Gamma = \left[\mathrm{A}, \mathrm{A}^2, \ldots, A^N\right]^{\mathrm{T}}, \tag{27}$$

$$\Upsilon = \begin{bmatrix} B & 0 & ... & 0 \\ AB & B & ... & 0 \\ \vdots & \vdots & \vdots & \vdots \\ A^{N-1}B & A^{N-2}B & ... & B \end{bmatrix}, \tag{28}$$

$$\Pi = [F, AF + F, ..., \sum_{j=0}^{N-1} A^j F]^{\mathrm{T}}. \tag{29}$$

The calculation burden of multi-step MPC strategy is greater than that of single step MPC, so delay compensation is very important. Therefore, it is necessary to make a one-step prediction of the current in advance based on Eq. (30) to replace the current measurement value $x_{dq}(k)$. It is worth noting that $s(k-1)$ is the optimal control input at the last moment. That is use $x_{dq}(k+1|k)$ to replace $x_{dq}(k)$.The predicted current output sequence(Eq. (26)) after considering delay compensation can be expressed as follows.

$$x_{dq}(k+1|k) = Ax_{dq}(k) + Bs(k-1) + F. \tag{30}$$

$$Y_{dq}^p = \Gamma x_{dq}(k+1|k) + \Upsilon S + \Pi. \tag{31}$$

Therefore, after considering delay compensation, the cost function the multi-step MPC can be designed as follows:

$$J = \left\| Y_{dq}^p - Y_{dq}^* \right\|_2^2 + \lambda \left\| WS - Es(k-1) \right\|_2^2, \tag{32}$$

where:

$$W = \begin{bmatrix} I & 0 & ... & 0 \\ -I & I & ... & 0 \\ 0 & -I & ... & 0 \\ \vdots & \vdots & \vdots & \vdots \\ 0 & 0 & ... & I \end{bmatrix}, E = \begin{bmatrix} I \\ 0 \\ 0 \\ \vdots \\ 0 \end{bmatrix}, \tag{33}$$

$$Y_{dq}^* = \left[\underbrace{x_{dq}^* \quad x_{dq}^* \quad \ldots \quad x_{dq}^* \quad x_{dq}^*}_{N} \right]. \tag{34}$$

As evident from Eq. (32), the first part of the cost function is used to evaluate predictive current tracking error, and the second part is used to evaluate the switching effort. In this

paper, the quadratic programming solver in Matlab is used to obtain the optimal solution of the cost function. This is a solver specially designed for solving quadratic objective functions with linear constraints. Specific use methods and notes can be obtained in Matlab help documentation.Before using the quadprog function in the solver to solve the cost function(32), we need to convert the value function into the following quadratic form.

$$J = \frac{1}{2}x^T Q x + \Xi(k)^T x, \tag{35}$$

where Q is the Hessian matrix and $\Xi(k)$ is a vector. Defining the following variables:

$$\Omega(k) = {Y_{dq}}^* - \Pi, \tag{36}$$

$$\xi(k) = \|\Gamma x_{dq}(k+1|k) - \Omega(k)\|_2^2 + \lambda \|Es(k-1)\|_2^2, \tag{37}$$

$$\Xi(k) = ((\Gamma x_{dq}(k+1|k) - \Omega(k|k))^{\mathrm{T}} \Upsilon - \lambda (Es(k-1))^{\mathrm{T}} W)^T, \tag{38}$$

$$Q = \Upsilon^{\mathrm{T}} \Upsilon + \lambda W^{\mathrm{T}} W. \tag{39}$$

The cost function can be cast into the following quadratic form:

$$J = S^T Q S + 2\Xi(k) S + c(k) \tag{40}$$

where

$$c(k) = \xi(k) - \Xi(k)^{\mathrm{T}} Q^{-1} \Xi(k). \tag{41}$$

Note that $c(k)$ is time varying, but is independent of the control variable S. The optimization problem after ignoring the independent term can be expressed as

$$S_{opt} = \arg\min_S \frac{1}{2} S^T Q S + \Xi(k)^T S \tag{42}$$

$$\text{s.t.} \quad x_{dq}(k+1|k) = A x_{dq}(k) + B s(k) + F, \tag{42a}$$

$$S_{opt}(i) \in [0,1], i = 1, 2, \cdots, 3N, \tag{42b}$$

$$\left\|Y_{dq}^*\right\|^2 \leq I_{dq\max}^2, \tag{42c}$$

where Eq.(42a) represents the equation constraint of discrete model, inequality Eq.(42b) represents control input constraint. Eq.(42c) is the inequality constraint of $d-q$ axis reference current with $\left\|Y_{dq}^*\right\|^2 = {Y_{dq}}^{*T} {Y_{dq}}^*$ and $I_{dqmax} = \sqrt{2} I_{max}$, where I_{max} represents the maximum rms current of PMLSM. Note that the S_{opt} is a vector with $3N$ elements, and contains the optimal solution from time $k+1$ to time $k+N$, and $S_{opt}(i)$ represent the i-th element of S_{opt}. Usually we take the first three elements as the optimal switching state, viz, (Abu-Ali et al. (2022))

$$s_{opt} = [S_{opt}(1), S_{opt}(2), S_{opt}(3)]^T. \tag{43}$$

NTSMC schemes for the speed control loop

In traditional motor control systems, outer-loop controllers usually adopts a proportional-integral (PI) control algorithm. Although PI controller is widely used owing to its mature technology and simple structure, its control performance can be questionable for the cases with unknown disturbances. Therefore, we design a novel controller by using NTSMC algorithm to replace the traditional PI controller. Additionally we designs a load observer to compensate the output of the above controller.

Design of the NTSMC strategy

Define the speed error as

$$e = v^* - v, \tag{44}$$

where v^* is reference speed. Based on Eq. (3), one has

$$\begin{cases} \dot{e} = \dot{v}^* - \dot{v} = -\frac{1}{M}\left(\frac{3}{2\tau}\pi n\varphi_f i_q - F_d - B_v v\right), \\ \ddot{e} = \ddot{v}^* - \ddot{v} = -\frac{1}{M}\left(\frac{3}{2\tau}\pi n\varphi_f \dot{i_q} - \dot{F}_d - B_v \dot{v}\right). \end{cases} \tag{45}$$

Generally, sampling frequency of a controller is much higher than the changing frequency of disturbance, hence disturbance can be regarded as a constant within a single sampling period (Lu et al. (2016, 2021)). Therefore, Eq. (45) can be modified as:

$$\begin{cases} \dot{e} = \dot{v}^* - \dot{v} = -\frac{1}{M}\left(\frac{3}{2\tau}\pi n\varphi_f i_q - F_d - B_v v\right), \\ \ddot{e} = \ddot{v}^* - \ddot{v} = -\frac{1}{M}\left(\frac{3}{2\tau}\pi n\varphi_f \dot{i_q} - B_v \dot{v}\right). \end{cases} \tag{46}$$

Let $u = \dot{i_q}$, $D = \frac{3}{2\tau M}\pi n\varphi_f$, and the non-singular sliding surface can be selected as follows:

$$\varpi = ke + \alpha e^{g/h} + \beta \dot{e}^{p/q}, \tag{47}$$

where k, α, β are all greater than zero, g, h, p, q are positive odd numbers; $1 < p/q < 2$ and $p/q < g/h$. The differentiation of non-singular fast terminal sliding mode surface can be obtained as follows:

$$\begin{aligned} \dot{\varpi} &= k\dot{e} + a\frac{g}{h}e^{g/h-1}\dot{e} + \beta\frac{p}{q}\dot{e}^{p/q-1}(-Du + \frac{B_v}{M}\dot{v}) \\ &= (k + a\frac{g}{h}e^{g/h-1})\dot{e} - \beta\frac{p}{q}\dot{e}^{p/q-1}Du + \frac{\beta B_v p}{qM}\dot{e}^{p/q-1}\dot{v}. \end{aligned} \tag{48}$$

Subsequently, the controller is designed as:

$$u = \frac{1}{D}(\frac{q}{\beta p}\dot{e}^{2-p/q}(k + \alpha\frac{g}{h}\dot{e}^{g/h-1}) + \frac{B_v\dot{v}}{M} + \frac{q}{\beta p}\dot{e}^{1-p/q}(\xi\mathrm{sgn}(\varpi) + \gamma\varpi)). \tag{49}$$

The reference current, namely i_q^*, generated by the sliding mode controller can be obtained by

$$i_q^* = \frac{1}{D}\int(\frac{q}{\beta p}\dot{e}^{2-p/q}(k + \alpha\frac{g}{h}\dot{e}^{g/h-1}) + \frac{B_v\dot{v}}{M} + \frac{q}{\beta p}\dot{e}^{1-p/q}(\xi\mathrm{sgn}(\varpi) + \gamma\varpi))dt, \tag{50}$$

where $\xi > 0$, and $\gamma > 0$.

Due to the time delay and the spatial lag, there is usually a certain amount of chattering around the sliding mode surface in practical applications. In order to suppress it, the function $f(\varpi)$ is defined as (Lu et al. (2016))

$$f(\varpi) = \begin{cases} \operatorname{sgn}(\varpi), |\varpi| \geq \Delta \\ \sin(\delta\varpi), |\varpi| < \Delta \end{cases}, \tag{51}$$

where $\delta = \pi/(2\Delta)$, and Δ is a boundary layer thickness. Hence, Eq. (50) can be rewritten as:

$$i_q^* = \frac{1}{D}\int (\frac{q}{\beta p}\dot{e}^{2-p/q}(k + \alpha\frac{g}{h}\dot{e}^{g/h-1}) + \frac{B_v\dot{v}}{M} + \frac{q}{\beta p}\dot{e}^{1-p/q}(\xi f(\varpi) + \gamma\varpi))dt. \tag{52}$$

To verify the stability of designed controller, the following Lyapunov function is selected:

$$V = \frac{1}{2}\varpi^2. \tag{53}$$

Based on Eqs. (48-52), the differentiation of non-singular terminal sliding mode surface can be expressed as:

$$\dot{\varpi} = k\dot{e} + a\frac{g}{h}e^{g/h-1}\dot{e} + \beta\frac{p}{q}\dot{e}^{p/q-1}(-Du + \frac{B_v}{M}\dot{v}) = -(\xi f(\varpi) + \gamma\varpi). \tag{54}$$

Differentiating V with respect to time, one has

$$\dot{V} = \varpi\dot{\varpi} = -(\varpi\xi f(\varpi) + \gamma\varpi^2). \tag{55}$$

Since $f(\varpi)$ is a piecewise function, it needs to be discussed in two cases. First, when $|\varpi| \geq \Delta$, $\dot{V} = \varpi\dot{\varpi} = -(\xi|\varpi| + \gamma\varpi^2)$. Due to $\xi > 0$ and $\gamma > 0$, it holds $\dot{V} \leq 0$. In the other case, i.e., $|\varpi| < \Delta$, $\dot{V} = \varpi\dot{\varpi} = -(\varpi\xi\sin(\delta\varpi) + \gamma\varpi^2)$. Due to $\xi > 0$, $\gamma > 0$, it can be derived that $\dot{V} \leq 0$. Hence, it can be concluded that $\dot{V} \leq 0$. Thus, the sliding mode controller designed in this paper is stable.

Design of the observer

In practice, the load changes of a motor greatly affect the closed-loop control performance. Hence, a NDO is considered to address this issue. It is assumed that the load dominates the disturbance term. From (6), the mechanical dynamic equation can be expressed as follow (Chen et al. (2015)):

$$\dot{x} = f(x) + g_1(x) + g_2(x)F_d, \tag{56}$$

where $x = v$, $f(x) = B_v v/M$, $g_1 = D * i_q$, $g_2 = -1/M$. According to Chen et al. (2015); Ding et al. (2020), the NDO can be designed as follow:

$$\begin{cases} \dot{z} = -l(x)g_2(x)z - l(x)\left[f(x) + g_1(x)u + g_2p(x)\right] \\ \hat{F}_d = z + p(x) \end{cases}, \tag{57}$$

where z represent the internal state, $\hat{F}_d$ is estimation of F_d and $p(x) = \int l(x)\dot{x}dt$. $l(x)$ is a crutial parameter for NDO, which determines the tracking speed and convergence accuracy of the observer. Let $l(x) = c$, which is a constant.

Define the observer error of NDO as follow:

$$e_d = F_d - \hat{F}_d. \tag{58}$$

Since the sampling frequency of the NDO is much larger than the changing frequency of the load, we hold that the disturbance remains unchanged within a sampling period, that is, $\dot{F}_d = 0$. Combine (3) and (57), we can obtain that

$$\begin{aligned}
\dot{e}_d &= \dot{F}_d - \dot{\hat{F}}_d \\
&= cxg_2(x)z + c\left[f(x) + g_1(x)u + g_2(x)cx\right] - c\dot{x} \\
&= -c\left[\dot{x} - g_2(x)z - f(x) - g_1(x)u - g_2(x)cx\right] \\
&= -c\left[f(x) + g_1(x)u + g_2F_d - g_2(x)z - f(x) - g_1(x)u - g_2(x)cx\right] \\
&= -c\left[g_2(x)F_d - g_2(x)\hat{F}_d\right] \\
&= -cg_2(x)e_d
\end{aligned} \tag{59}$$

To verify the stability of designed observer, the following Lyapunov function is selected:

$$V_2 = \frac{1}{2}e_d^2 \tag{60}$$

Combining Eq.(59), we can obtain differential expression of V_2 is as follows

$$\dot{V}_2 = e_d\dot{e}_d = -cg_2(x)e_d^2. \tag{61}$$

Due to $g_2(x) = -1/M < 0$, as long as $c < 0$, it can be guaranteed that $\dot{V}_2 < 0$. According to the Lyapunov stability theory, the designed observer is stable. In the observer design, faster tracking speed can be achieved by selecting a smaller value of c. However, if c is too small, the observation curve will have large fluctuations, which is not suitable for the starting period. On the other hand, if c is too large, the observer cannot track the disturbance in time. Through repeated debugging in simulation and experiment, it is found that when $c = -200$, the observation speed and observation accuracy of the observer can meet the control requirements of the system.

After proving the stability of NTSMC and NDO respectively, we need to discuss whether the stability of the entire control system can still be guaranteed after the disturbance compensation is obtained. Define a global Lyapunov equation consisting of a sliding mode surface function ϖ and a perturbation tracking error function e_d.

$$V = V_1 + V_2 = \frac{1}{2}\varpi^2 + \frac{1}{2}e_d^2. \tag{62}$$

Differentiating V with respect to time, one has

$$\dot{V} = \dot{V}_1 + \dot{V}_2 = \dot{\varpi}\varpi + \dot{e_d}e_d. \tag{63}$$

Based on Eq.(55) and Eq.(61), when $c < 0$, $\xi > 0$, and $\gamma > 0$, it can be ensure $\dot{V} <= 0$. Thus, according to Lyapunov stability theory we can know the whole control system is asymptotically stable.

Finally, the load observer is utilized to compensate the output of the sliding mode controller designed for outer loop. The q-axis reference current is obtained as follows

$$\begin{aligned} i_q^* =& g_m \hat{F}_d + \frac{1}{D}\int (\frac{q}{\beta p}\dot{e}^{2-p/q}(k + \alpha\frac{g}{h}\dot{e}^{g/h-1}) \\ &+ \frac{B_v\dot{v}}{M} + \frac{q}{\beta p}\dot{e}^{1-p/q}(\xi f(\varpi) + \gamma\varpi))dt, \end{aligned} \tag{64}$$

where $g_m = \frac{1}{DM}$ is the feedforward gain.

Simulations and experiments

Simulations and comparative analysis

The simulations in this section are carried out in Matlab. In order to show the advantages of the proposed algorithm, the calculation time T_c of the traditional traversal method and the proposed one under different predictive horizons are demonstrated in Table 1. It is shown that there is no much difference of the computing time when the predictive horizon $N = 1$. However, when the predictive horizon $N = 2$, the computing time employing the traditional multi-step predictive control algorithm is about twice that of the proposed algorithm. It is worth mentioning that the traditional approach may not be applicable when the predictive horizon length $N \geq 3$, since the computing time approximates the sampling period.

Table 1. Computing time comparisons of different multi-step MPC algorithms.

N	T_c/μs	
	traversal method	quadratic optimization method
1	2.8	2.9
2	13.4	6.8
3	$T_c > T_s$	16.9
...	...	...

To validate the control performance of the proposed strategy, two sets of simulations are conducted. In the following simulations and experiments, the predictive horizon N is set as 3. Moreover, the parameters of PMLSMs are given in Table 2. The switching devices in the inverter are insulted-gate bipolar transistors (IGBTs) with operational frequency of 10 kHZ and dc-link voltage is adjusted at 400V. According to method proposed in Ding et al. (2020), we designed the gains of PI controller to ensure its rationality and scientificity. The PI's control gain k_{sp} and k_{si} in speed outer loop can be designed as $k_{sp} = 2\xi\omega_s/D, k_{si} = \omega_s^2/D$, where k_{sp} and k_{si} represent the proportional

gain and integral gain respectively, ω_s is bandwidth and ξ is damping coefficient. In the Simulink and experiment, ω_s and ξ are 40 and 0.7 respectively, so the control gain are $k_{sp} = 19$, $k_{si} = 184$. The parameters of NTSMC in this paper are selected as follows: $k = 2$, $\alpha = 1$, $\beta = 1$, $g = 5$, $h = 3$, $p = 7$, $q = 5$, $\xi = 100$, and $\gamma = 450$. The load profile is described as $F_L(k) = 40N$ in our simulations. In this paper, the NDO'parameter $c = -200$.

Table 2. Parameters of the PMLSM in simulations.

Parameters	Variable name	Value
Stator resistance[Ω]	R_s	9.7
Stator Inductance[mH]	L	43.3
Mover mass[kg]	M	3.2
Friction coefficient[N·s/m]	B_v	0.5
pole-pitch[mm]	τ	27
permanent magnet flux linkage[Wb]	$flux$	0.165
number of pole pairs	n	2
nominal speed[m/s]	v	1

To demonstrate the control performance of the proposed method in this paper, we compare it with the method proposed (PI_MPC) in Zhang et al. (2016) and SMC_PI based new sliding mode approach low proposed in Wang and Wei (2019) respectively. From the Fig. 2, we can conclude that the simulation results of the method proposed in this paper and the above two methods for comparison, including the speed curve, a-phase current curve and thrust force curve. First, the following conclusions can be drawn from Fig. 2(e). Even if the disturbance compensation brought by NDO is not considered, the speed overshoot and absolute speed drop (ASD) of the proposed method in this paper, are 7.1% and 0.018m/s respectively, which are smaller than other comparison method. This shows that the speed outer loop controller ,NTSMC, designed in this paper has a good dynamic performance.

In addition, it can be seen from the figure that the proposed method also outperforms the proposed methods in Zhang et al. (2016) and Wang and Wei (2019) in terms of current THD and thrust ripple. This is mainly attributed to the proposed multi-step CCS-MPC algorithm for current inner loop. It is also worth noting that when the load changes abruptly (t=0.5s), the access to NDO can reduce the ASD of the three methods mentioned above, especially the PI_MPC has the most obvious improvement, from 0.058m/s to 0.022m/s, after getting the disturbance compensation. As show in Fig. 2(e) and 2(f), it can be seen that the ASD index of the NTSMC_CCS-MPC method is reduced by about 27.8% after considering the disturbance compensation. The above simulation results show that NDO can improve the robustness of the system.

Furthermore, in order to reveal the advantages of the NTSMC_CCS-MPC proposed in this paper, the steady state performance indexes such as maximum error(ME), mean absolute error(MAE), and root mean squared error(RMSE) are evaluated.The

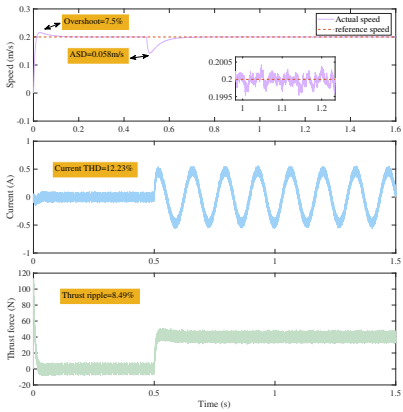

(a) without NDO: PI_MPC proposed in Zhang et al. (2016).

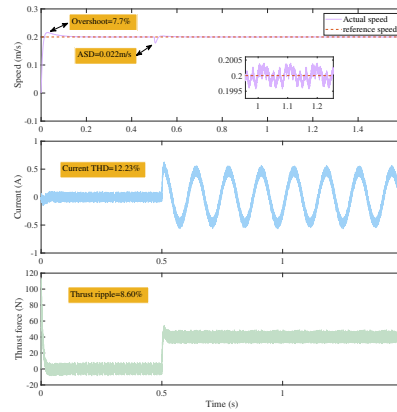

(b) with NDO: PI_MPC proposed in Zhang et al. (2016).

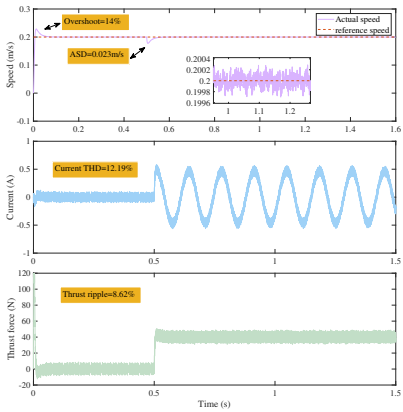

(c) without NDO: SMC_PI proposed in Wang and Wei (2019).

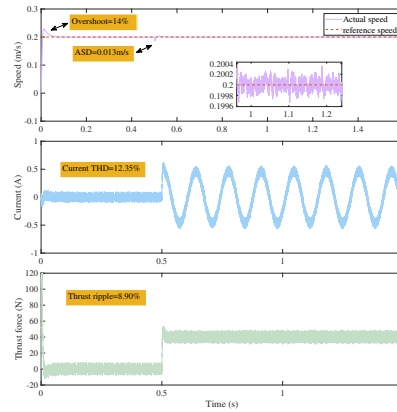

(d) with NDO: SMC_PI proposed in Wang and Wei (2019).

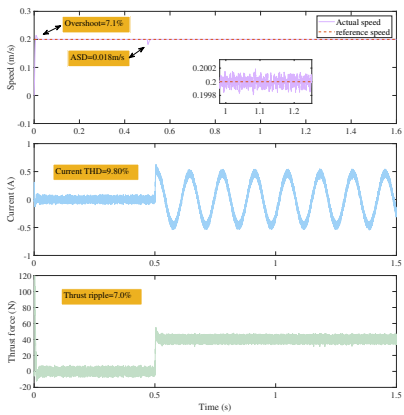

(e) without NDO: NTSMC_CCSMPC proposed in this paper.

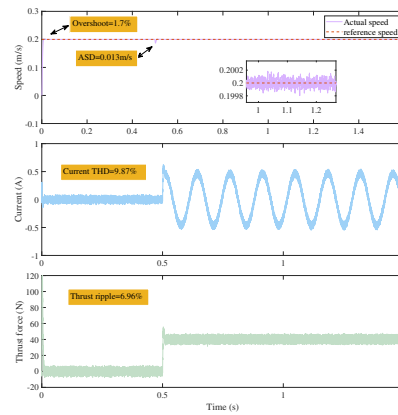

(f) with NDO: NTSMC_CCSMPC proposed in this paper.

Figure 2. Simulation results of speed, phase current, thrust.

relevant informations are given in Fig. 3. It can be summaried that the error indexes of NTSMC_CCS-MPC are better than comparative solutions. Therefore, it can be concluded that the proposed scheme in the paper has better steady-state performance. In conclusion, the simulation results show that the proposed algorithm has relatively satisfactory dynamic and steady-state performance.

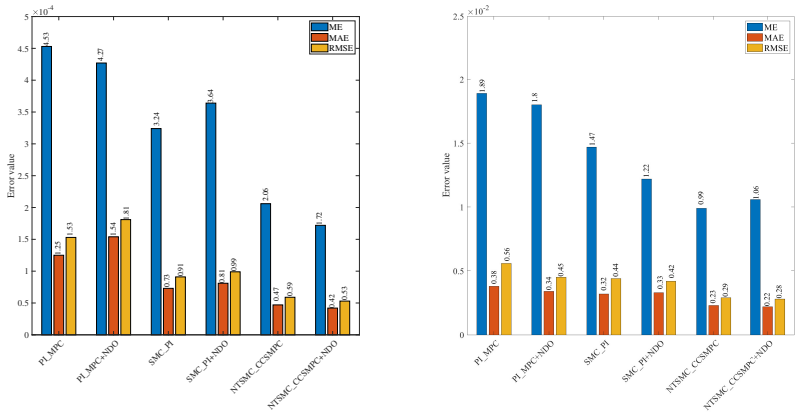

Figure 3. The speed error index: (a) simulation results. (b) experimental results.

Remark 2

The simulation results show that NDO can reduce the speed drop caused by sudden load changes and improve the robustness of the system. It is worth noting that when the load remains constant, the steady-state performance improvement brought by NDO is limited. Speed error, current THD, and thrust ripple have little change compared to before.

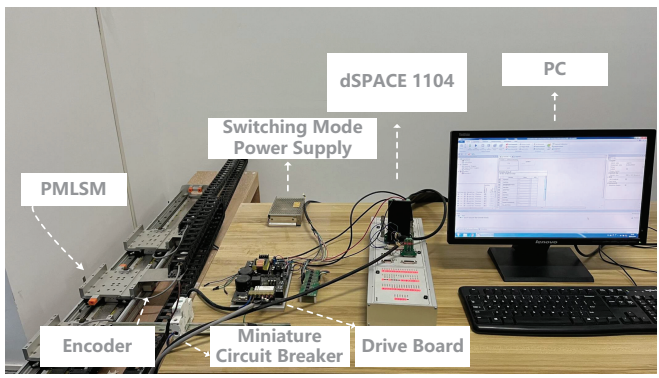

Figure 4. The PMLSM experimental platform.

Experiments and comparative analysis

To verify the practical effectiveness of the proposed approach, experiments are further conducted on a dSPACE-based platform as shown in Fig. 4. The experimental platform consists of PMLSM, a driver board, an incremental encoder, and so on. Two Hall sensors are provided on the driver board, which are used to detect the current information of the PMLSM. In addition, the incremental encoder provides coded information through which the position, speed, and angle information of the PMLSM can be obtained. These feedback signals are indispensable in the controller design. It can be said that the accuracy of above signal directly affects the control performance. The relevant parameters of the PMLSM are still the ones listed in Table 2. Moreover, all controller parameters keep the same with those used in simulations.

Fig. 5 shows the experimental results of the method proposed in this paper and the above two methods for comparison, including the speed curve, a-phase current curve and thrust force curve. The experimental results are demonstrated in Fig. 5 and Table. 3 , where Fig. 5(a) (c) (e) and Fig. 5(b) (d) (f) respectively show the experimental results of the above approchs under the conditions of whether or not disturbance compensation is considered. It is noticed that compared with the other two methods, the speed overshoot of the method proposed in this paper is reduced by 16.8% and 18% respectively. When the speed of PMLSM reaches a steady state, its speed fluctuation is relatively smaller than the other two methods. It is worth emphasizing that the speed error of the method proposed in this paper is minimal without considering disturbance compensation. The specific error data can be obtain in Fig. 3(b). In addition, it can be seen from the Table 3 that the proposed method also outperforms the proposed methods in Zhang et al. (2016) and Wang and Wei (2019) in terms of current THD and thrust ripple.

When both scenarios considers the load observation, due to the lack of relevant experimental equipment, it is temporarily impossible to verify the scene of sudden load changes in the experiment, similar to the simulation results, the steady-state performance improvement brought by NDO is limited.

Remark 3

Through the comparison of simulation and experimental results, it can be seen that the current and thrust fluctuations in the experiment are much larger than the results in the simulation, which may be caused by the following reasons:

(i) The experimental platform is old, and the processing power of dSPACE1104 core processor is limited. When the control algorithm is more complex, the sampling frequency can only be set at 5kHz.
(ii) In order to protect the inverter, a dead time is usually set. The dead time set by the three-phase two-level inverter used in this experiment platform is 5us, which is greater than the dead time required by some high-performance inverters, which may cause distortion of the three-phase current.

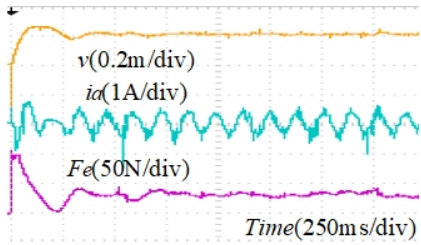

(a) without NDO: PI_MPC proposed in Zhang et al. (2016).

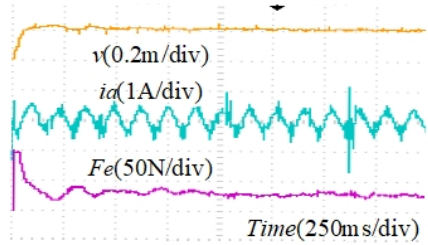

(b) with NDO: PI_MPC proposed in Zhang et al. (2016).

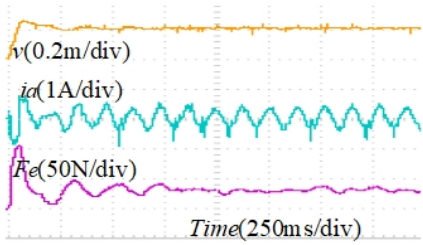

(c) without NDO: SMC_PI proposed in Wang and Wei (2019).

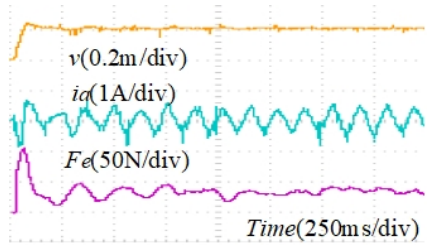

(d) with NDO: SMC_PI proposed in Wang and Wei (2019).

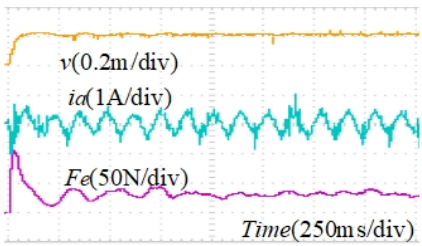

(e) without NDO: NTSMC_CCSMPC proposed in this paper.

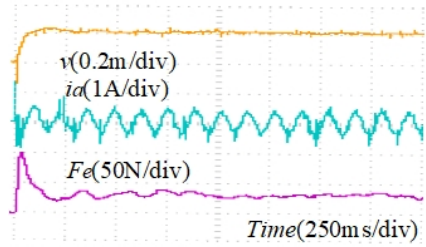

(f) with NDO: NTSMC_CCSMPC proposed in this paper.

Figure 5. Experimental results of speed, phase current, thrust.

Table 3. Experimental performance evaluation.

	Overshoot(%)	THD(%)	Thrust ripple(%)
PI_MPC	27.1	20.03	15.4
PI_MPC+NDO	15.2	22.17	13.8
SMC_PI	28.3	19.58	15.9
SMC_PI+NDO	26.7	19.96	16.5
NTSMC_CCSMPC	10.3	19.2	15.5
NTSMC_CCSMPC +NDO	12.5	18.47	14.6

Conclusion

This paper proposes an NTSMC-based CCS-MPC method to control a PMLSM. Specifically, the NTSMC approach is employed in the controller design for the speed control loop of the PMLSM. A load observer is further designed to improve the overall control performance. The effectiveness of the proposed approach is verified through both simulations and experiments. To demonstrate the control performance of the proposed method in this paper, we compare it with the method proposed (PI_MPC) in Zhang et al. (2016) and SMC_PI based new sliging mode approach low proposed in Wang and Wei (2019) respectively. The simulation and experimental results show that the NTSMC-based CCS-MPC approach offers smaller speed fluctuations, with great anti-disturbance capability.

Declaration of conflicting interests

The author(s) declared no potential conflicts of interest with respect to the research, authorship, and/or publication of this article.

Acknowledgements

This work was supported in part by the National Natural Science Foundation of China (Grant No.62222307, No.61973140) and the Natural Science Foundation of Jiangsu Province (Grant No.BK20211235, No.BK20210475).

References

Abu-Ali M, Berkel F, Manderla M, Reimann S, Kennel R and Abdelrahem M (2022) Deep learning-based long-horizon mpc: Robust, high performing and computationally efficient control for pmsm drives. *IEEE Transactions on Power Electronics* .

Ahmed AA, Koh BK and Lee YI (2018) A comparison of finite control set and continuous control set model predictive control schemes for speed control of induction motors. *IEEE Transactions on Industrial Informatics* 14(4): 1334–1346.

Ahmed AA, Koh BK, Park HS, Lee KB and Lee YI (2017) Finite-control set model predictive control method for torque control of induction motors using a state tracking cost index. *IEEE Transactions on Industrial Electronics* 64(3): 1916–1928.

Candelo-Zuluaga C, Riba JR and Garcia A (2021) Pmsm parameter estimation for sensorless foc based on differential power factor. *IEEE Transactions on Instrumentation and Measurement* 70: 1–12.

Chen SY and Liu TS (2017) Intelligent tracking control of a pmlsm using self-evolving probabilistic fuzzy neural network. *IET Electric Power Applications* 11(6): 1043–1054.

Chen WH, Yang J, Guo L and Li S (2015) Disturbance-observer-based control and related methods—an overview. *IEEE Transactions on industrial electronics* 63(2): 1083–1095.

Ding B, Xu D, Jiang B, Shi P and Yang W (2020) Disturbance-observer-based terminal sliding mode control for linear traction system with prescribed performance. *IEEE Transactions on transportation electrification* 7(2): 649–658.

Englert T and Graichen K (2018) Nonlinear model predictive torque control of pmsms for high performance applications. *Control Engineering Practice* 81(1): 43–54.

Guo Q, Pan T, Liu J and Chen S (2021) Explicit model predictive control of permanent magnet synchronous motors based on multi-point linearization. *Transactions of the Institute of Measurement and Control* 43(12): 2872–2881.

Huang W, Zhu X, Zhang H and Hua W (2023) Generalized fault-tolerant model predictive control of five-phase pmsm drives under single/two open-switch faults. *IEEE Transactions on Industrial Electronics* .

Jiang X, Yang Y, Fan M, Ji A, Xiao Y, Zhang X, Zhang W, Garcia C, Vazquez S and Rodriguez J (2022) An improved implicit model predictive current control with continuous control set for pmsm drives. *IEEE Transactions on Transportation Electrification* 8(2): 2444–2455.

Jon R, Wang Z, Luo C and Jong M (2017) Adaptive robust speed control based on recurrent elman neural network for sensorless pmsm servo drives. *Neurocomputing* 227: 131–141.

Koiwa K, Kuribayashi T, Zanma T, Liu KZ and Wakaiki M (2019) Optimal current control for pmsm considering inverter output voltage limit: model predictive control and pulse-width modulation. *IET Electric Power Applications* 13(12): 2044–2051.

Kommuri SK, Park Y and Lee SB (2021) Online compensation of mechanical load defects with composite control in pmsm drives. *IEEE/ASME Transactions on Mechatronics* 26(3): 1392–1400.

Lu E, Li W, Wang S, Zhang W and Luo C (2021) Disturbance rejection control for pmsm using integral sliding mode based composite nonlinear feedback control with load observer. *ISA transactions* 116: 203–217.

Lu X, Lin H and Han J (2016) Load disturbance observer-based control method for sensorless pmsm drive. *IET Electric Power Applications* 10(8): 735–743.

Nguyen AT, Ryu SW, Rehman AU, Choi HH and Jung JW (2021a) Improved continuous control set model predictive control for three-phase cvcf inverters: Fuzzy logic approach. *IEEE Access* 9: 75158–75168.

Nguyen ND, Nam NN, Yoon C and Lee YI (2021b) Speed sensorless model predictive torque control of induction motors using a modified adaptive full-order observer. *IEEE Transactions on Industrial Electronics* 69(6): 6162–6172.

Shi Z, Wang Y and Ji Z (2016) Bias compensation based partially coupled recursive least squares identification algorithm with forgetting factors for mimo systems: Application to pmsms. *Journal of the Franklin Institute* 353(13): 3057–3077.

Siami M, Khaburi DA, Rivera M and Rodríguez J (2017) A computationally efficient lookup table based fcs-mpc for pmsm drives fed by matrix converters. *IEEE Transactions on Industrial Electronics* 64(10): 7645–7654.

Wang A and Wei S (2019) Sliding mode control for permanent magnet synchronous motor drive based on an improved exponential reaching law. *IEEE access* 7: 146866–146875.

Wang F, He L, Kang J, Kennel R and Rodríguez J (2022) Adaptive model predictive current control for pmlsm drive system. *IEEE Transactions on Industrial Electronics* 70(4): 3493–3502.

Wang M, Yang R, Zhang C, Cao J and Li L (2018) Inner loop design for pmlsm drives with thrust ripple compensation and high-performance current control. *IEEE Transactions on Industrial*

Electronics 65(12): 9905–9915.

Wang MS and Tsai TM (2017) Sliding mode and neural network control of sensorless pmsm controlled system for power consumption and performance improvement. *Energies* 10(11): 1780.

Xu D, Ding B, Jiang B, Yang W and Shi P (2022) Nonsingular fast terminal sliding mode control for permanent magnet linear synchronous motor via high-order super-twisting observer. *IEEE/ASME Transactions on Mechatronics* 27(3): 1651–1659.

Xu D, Zhang W, Shi P and Jiang B (2019) Model-free cooperative adaptive sliding-mode-constrained-control for multiple linear induction traction systems. *IEEE Transactions on Cybernetics* 50(9): 4076–4086.

Yin P, Guo J and He H (2022) Backstepping sliding-mode techniques in current control of polymer electrolyte membrane fuel cell. *Control Engineering Practice* 124: 105188.

Zhang X, Hou B and Yang M (2016) Deadbeat predictive current control of permanent-magnet synchronous motors with stator current and disturbance observer. *IEEE Transactions on Power Electronics* 32(5): 3818–3834.

Zhao K, Yin T, Zhang C, He J, Li X, Chen Y, Zhou R and Leng A (2019) Robust model-free nonsingular terminal sliding mode control for pmsm demagnetization fault. *IEEE Access* 7: 15737–15748.